

THE EFFECTS OF NATURAL VARIABILITY AND CLIMATE CHANGE ON THE RECORD LOW SUNSHINE OVER JAPAN DURING AUGUST 2017

CHIHARU TAKAHASHI, HIDEO SHIOGAMA, YUKIKO IMADA, YU KOSAKA, MASATO MORI, MIKI ARAI, YUICHI KAMAE, AND MASAHIRO WATANABE

The record low sunshine over Japan during August 2017 was mainly attributed to a blocking high and Pacific–Japan pattern. Anthropogenic warming and decaying El Niño contributed to an increase in the probability of occurrence.

INTRODUCTION. Early August in 2017 had record poor sunshine in northern Japan with anomalously cool and rainy conditions, which damaged agriculture and the economy. There was very low sunshine for one week at several observation sites on the Pacific side of northern Japan, the longest duration in July and August since 1961 (Figs. 1a,b). Observational analysis indicates that the prolonged cloudy days were caused by cold northeasterly winds in that region (Fig. 1d; see also Figs. ES1a and ES1b in the online supplemental information). These cold winds are associated with two possible factors. One is the surface Okhotsk high associated with a blocking high over East Siberia (Figs. 1c–e). The Okhotsk high often causes anomalously cold summers in northern Japan (Kodama 1997; Nakamura and Fukamachi 2004). The prominent Okhotsk high in August 2017 formed in association with the propagation of a stationary Rossby wave in the middle-upper troposphere from Europe through East Siberia (Fig. ES1c), as shown by Sato and Takahashi

(2007). The other possible factor of the cold winds is the Pacific–Japan (PJ) teleconnection pattern (Nitta 1987; Kosaka and Nakamura 2006, 2010) induced by anomalously suppressed convective activity over the Philippine Sea (Fig. 1e; see also Figs. ES1b,d,e) associated with a northward-propagating intraseasonal oscillation from the tropics (Figs. ES1f,g). In advance of the event, tropical cyclones (T1705 and T1711) developed as a part of the PJ teleconnection and could have provided an initial moist condition in Japan. The PJ pattern and anomalous Okhotsk high often co-occur (Wakabayashi and Kawamura 2004; Hirota and Takahashi 2012), and the resultant tripolar pattern of atmospheric circulation has been known to cause sunshine deficits such as that observed in August 2017 (Figs. ES1h,i).

It has been suggested that greater anthropogenic warming in the Far East land area than the surrounding ocean intensifies the anticyclonic circulation throughout the troposphere over eastern Siberia and the Okhotsk Sea (Kimoto 2005; Arai and Kimoto 2008; Kamae et al. 2014). The intensified anticyclone leads to strengthened easterly winds into northern Japan (Fig. ES1j). Geopotential height at 500 hPa (Z_{500}) and its deviation from the zonal mean (Z'_{500}) have an increasing trend of 7.2 and 2.1 m decade⁻¹, respectively, over eastern Siberia and the sea of Okhotsk (orange box in Fig. 1e) in July–August for 1961–2017 (Fig. ES1j). Sunshine duration has significantly decreased with a trend of -0.19 h month⁻¹ decade⁻¹ (Fig. 1b). Therefore, we can expect that anthropogenic warming has influenced the likelihood of the unusual blocking and Okhotsk high, which led to the 2017 extreme event.

Apart from the human influence, seasonal weather in Japan is strongly influenced by atmospheric variability forced by sea surface temperature (SST) variation in the tropics such as El Niño–Southern Oscillation (ENSO; Fig. ES1k). Although La Niña was gradually

AFFILIATIONS: TAKAHASHI, ARAI, AND WATANABE—Atmosphere and Ocean Research Institute, The University of Tokyo, Chiba, Japan; SHIOGAMA—Center for Global Environmental Research, National Institute for Environmental Studies, Tsukuba, Japan; IMADA—Meteorological Research Institute, Japan Meteorological Agency, Tsukuba, Japan; KOSAKA AND MORI—Research Center for Advanced Science and Technology, The University of Tokyo, Tokyo, Japan; KAMAE—Faculty of Life and Environmental Sciences, University of Tsukuba, Tsukuba, Ibaraki, Japan

CORRESPONDING AUTHOR: Chiharu Takahashi, chiha@aori.u-tokyo.ac.jp

DOI:10.1175/BAMS-D-18-0107.1

A supplement to this article is available online (10.1175/BAMS-D-18-0107.2)

© 2018 American Meteorological Society

For information regarding reuse of this content and general copyright information, consult the [AMS Copyright Policy](#).

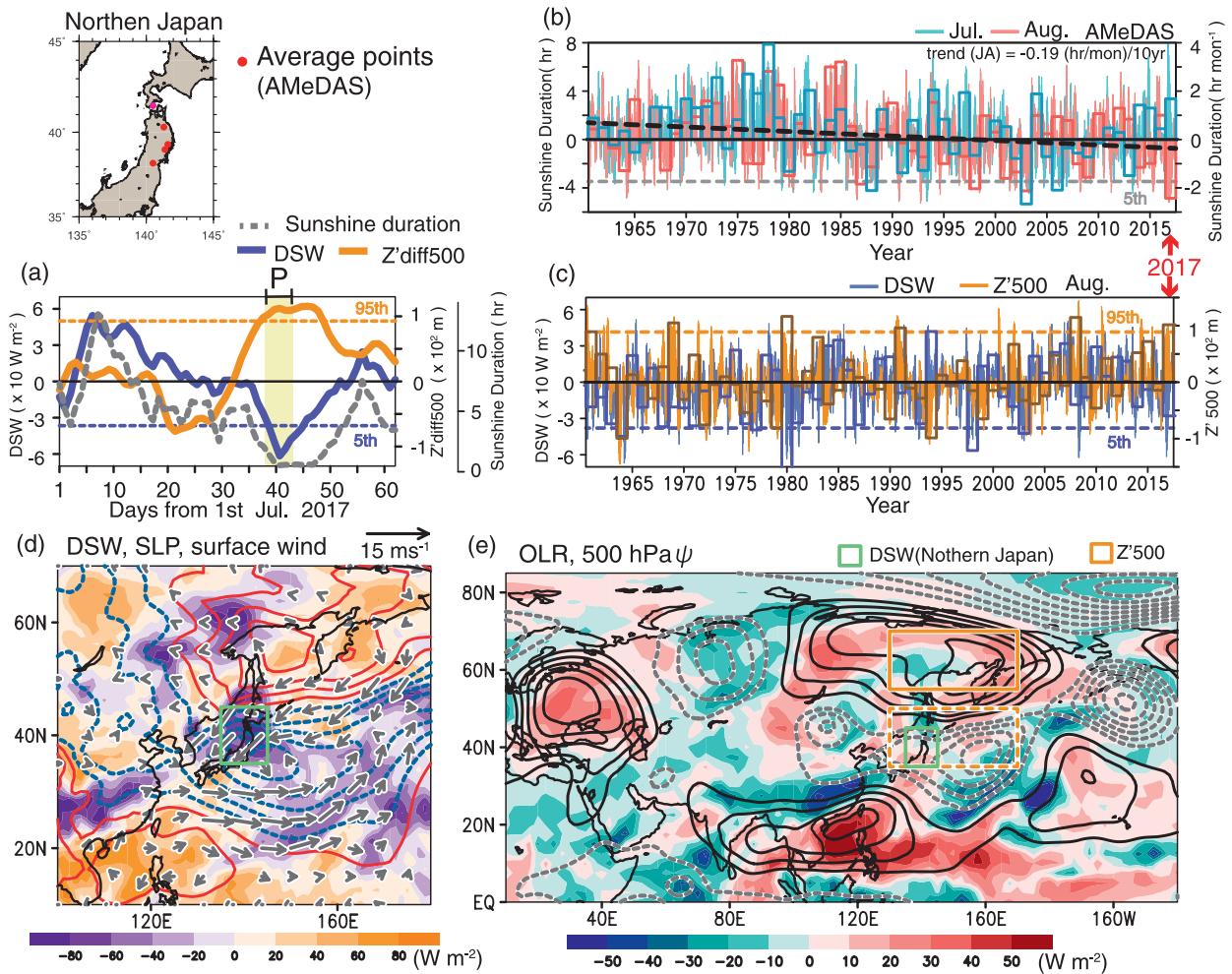


FIG. 1. (a) Time series of observed sunshine duration (gray) averaged at five observations sites (red circles in map of Japan) and anomalies of DSW (purple) over northern Japan (35° – 45° N, 135° – 145° E, green boxes in Figs. 1d,e) and $Z'_{diff} 500$ (difference in $Z' 500$ between orange and dashed boxes in Fig. 1e) in July–August 2017. (b) As in (a), but for sunshine duration in July (blue) and August (pink). (c) As in (a) but anomalies of $Z' 500$ over East Siberia and the Okhotsk Sea (solid box in Fig. 1e) and DSW in August for 1961–2017. The shading in (a) indicates the analysis period P (8–12 August). In (b) and (c), curves show 5-day running mean anomalies (with the axis in the left) and bars indicate monthly mean (the right axis). Also shown are observed patterns of the 5-day mean anomalies during the period P in (d) DSW (shading), sea level pressure (contours; 1.0-hPa interval), and surface winds (vectors) and (e) OLR (shading) and 500-hPa streamfunction (contours; $2 \times 10^6 \text{ m}^2 \text{ s}^{-1}$ interval). Dashed contours indicate negative anomalies.

developing in August 2017, the Niño-3.4 SST anomaly was still positive (about 0.26°C) like El Niño in July (Fig. ES2a), which potentially contributed to the development of the PJ pattern. Thus, we examine the contributions of anthropogenic warming and ENSO on the occurrence of the extreme low sunshine event in northern Japan in early August 2017 using an atmospheric general circulation model (AGCM).

METHODS. We have performed several sets of 100-member ensemble simulations for 2017 using the AGCM of MIROC5 (T85L40, Watanabe et al. 2010). Each member was started from different initial condi-

tions. ALL is the all-forcing run forced by the observed historical SST and sea ice derived from the HadISST dataset (Rayner et al. 2003). NAT1 and NAT2 are natural forcing runs driven by detrended HadISST based on 1870–2012 linear trends (NAT1; Christidis and Stott 2014) and by removing the anthropogenic changes in SST/sea ice based on attribution experiments from phase 5 of the Coupled Model Intercomparison Project (CMIP5) (NAT2; D. Stone and P. Pall 2017, unpublished manuscript: http://portal.neresc.gov/c20c/pub/StoneDA_PallP_2017.pdf). Details of ALL, NAT1, and NAT2 are described in Shiogama et al. (2013, 2014). ALLnoENSO is the same as ALL, but the monthly SST

anomalies regressed onto Niño-3.4 SST anomaly have been subtracted (Takahashi et al. 2016) in order to suppress the influence of ENSO in 2017. The SSTs that drive each experiment are shown in Fig. ES2. We have also performed a 10-member long-term ALL experiment, called ALL-LNG for 1949–2016, to define a threshold of the event. We used the daily JRA-55 reanalysis dataset (Kobayashi et al. 2015; Harada et al. 2016), outgoing longwave radiation (OLR) from NOAA (Liebmann and Smith 1996), and surface observations from the Automated Meteorological Data Acquisition System (AMeDAS) by the Japan Meteorological Agency.

Since MIROC5 does not provide sunshine duration diagnostics, we employ a surface downward solar radiation (DSW) index averaged over northern Japan (35°–45°N, 135°–145°E; green box in Figs. 1d,e) as a proxy, which is the same approach as in Christidis et al. (2016). Observed sunshine duration is highly correlated (at 0.76) with the DSW index in July–August for 1961–2017 based on JRA-55. The extreme event with very low sunshine duration is defined as the 5-day period of 8–12 August 2017 (indicated as “P” in Fig. 1a) centering around the minimum index day, when the DSW index fell outside the 5th percentile (Figs. 1a,c) based on the 5-day running-mean statistics for July–August of 1961–2017.

The Z'_{500} anomaly averaged over eastern Siberia and the Okhotsk Sea (orange box in Fig. 1e) also exceeds the 95th percentile (Fig. 1c). We assess the relative contribution of anthropogenic forcing and ENSO to the occurrence of the 2017 extreme event by estimating the fraction of attributable risk (FAR; Allen 2003), defined as $1 - (P_0/P_1)$, where P_1 and P_0 are probabilities exceeding a given threshold in ALL and NAT1/NAT2/ALLnoENSO simulations (each 100-member ensemble), respectively, and estimated based on probability density functions (PDFs) of the mean value for the period P . The threshold in each index is defined based on PDFs of 5-day running mean anomalies estimated from the 10-member ensemble of ALL-LNG for July–August 1961–2016. The best estimate (50th percentile) and 95% confidence interval (CI) of the probabilities are estimated through the bootstrap random resampling (each 1000 samples).

RESULTS. The observed DSW index averaged for the period P is -61.8 W m^{-2} (Fig. 2a). This value corresponds to the 0.3th percentile of the 5-day running mean index in July–August for the recent 57 years. Therefore, we adopt the first percentile (-75.0 W m^{-2}) as the threshold of the DSW index in ALL-LNG run. The best estimate in occurrence probability (95% CI) of the extreme DSW index that falls below the thresh-

old is 1.3% (0.0–3.4%), 0.17% (0.0–0.51%), 0.046% (0.0–0.40%), and 0.11% (0.0–0.40%) for ALL, NAT1, NAT2, and ALLnoENSO, respectively (Fig. 2a). The estimated FAR_{ANTH} (anthropogenic effect) and FAR_{ENSO} (ENSO effect) is 0.89–0.97 and 0.90, respectively. These results indicate that the anthropogenic warming contributed to increase of the chance of the 2017 extreme low sunshine by 7.7–29 times, suggesting that this event would hardly have happened without human influence. Besides, it is suggested that ENSO acted to raise the chance by about 12 times.

Ensemble-mean differences between ALL and NAT1/NAT2 can represent influence of anthropogenic forcing on the 2017 event, forced by SSTs (Figs. ES2c,d). The changes in Z'_{500} due to anthropogenic effect show enhanced anticyclonic circulation with lower-tropospheric warming in the extratropics covering eastern Siberia and the Okhotsk Sea (Fig. 2c and Fig. ES3a) and anomalous cyclonic circulation in the ocean to the east of Japan, which is consistent with previous studies (e.g., Kamae et al. 2014). These changes are similar to the ensemble-mean trends in ALL-LNG in July–August 1961–2017 (Fig. ES3b). The composite of extreme DSW members (below the second percentile) in ALL well represents the tripolar circulation pattern as in observations, with significantly weaker amplitudes in NAT1/NAT2 (Figs. ES3c–h).

We also evaluate likelihood of the extreme Okhotsk high related to the blocking ($Z'_{\text{diff}500}$), which is defined as difference of Z'_{500} anomalies between the eastern Siberia–Okhotsk sea sector (55°–70°N, 130°–170°E) and the area to its south (35°–50°N, 130°–170°E). The observed $Z'_{\text{diff}500}$ anomaly averaged in the period P is 112.3 m (Figs. 1a and 2b), corresponding to 97.2th percentile of 5-day running mean in July–August for the recent 57 years. The threshold of $Z'_{\text{diff}500}$ is thus defined as 107.0 m, which is equivalent to the 97th percentile in ALL-LNG. The best estimate (95% CI) in occurrence probability of extreme $Z'_{\text{diff}500}$ exceeding this threshold is 5.5% (2.3–9.3%), 2.2% (0.89–4.3%), 1.7% (0.41–3.4%), and 3.3% (1.0–6.5%) for ALL, NAT1, NAT2, and ALLnoENSO, respectively (Fig. 2b). The estimated FAR_{ANTH} and FAR_{ENSO} are 0.57–0.70 and 0.39, respectively. The results suggest that the anthropogenic warming contributed to raise the occurrence probability of the 2017 extreme Okhotsk high by 2.5–3.2 times, whereas ENSO influence was weaker (1.7 times).

The impact of ENSO in 2017 is represented by the difference of ensemble means between ALL and ALLnoENSO (Fig. 2d), which feature a teleconnection pattern similar to that occurs in July–August for El Niño years (Fig. ES1k). The decaying El Niño signal remained

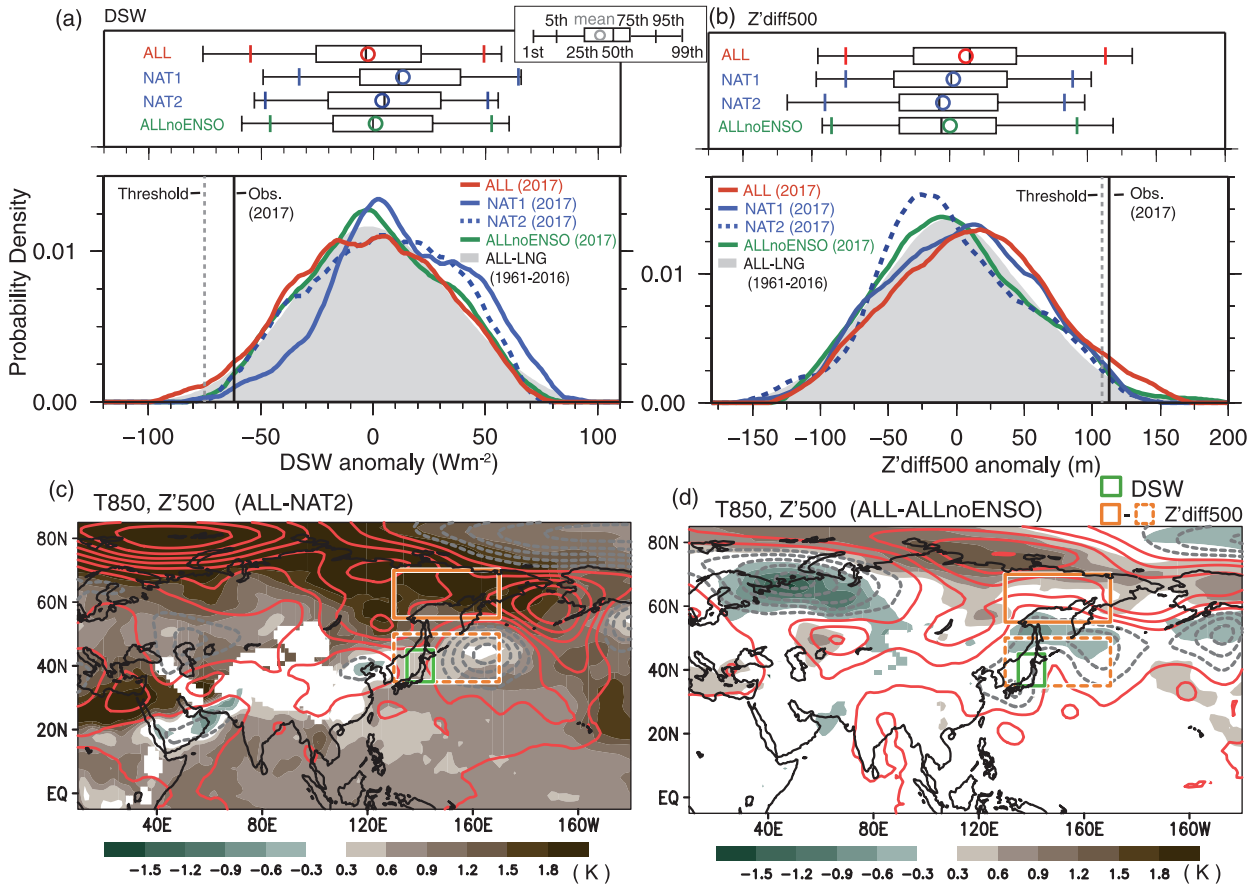


FIG. 2. (a),(b) Box-and-whisker plots and PDFs of (a) 5-day (the period P) average DSW anomalies over northern Japan (green boxes in Figs. 2c,d) and (b) $Z'_{diff500}$ anomalies (difference in $Z'500$ anomalies between orange solid and dashed boxes in Figs. 2d,e) in the 2017 event for ALL (red), NAT1 (blue solid), NAT2 (blue dashed), ALLnoENSO (green), and 5-day running mean anomalies in ALL-LNG for July–August, 1961–2016 (shading). The black and gray dashed lines indicate the 2017 observed anomalies and threshold, respectively. (c) Ensemble mean difference in 5-day average 850-hPa temperature (shading) and $Z'500$ anomalies (contours; 5-m interval with negative dashed) between ALL and NAT2. (d) As in (c), but for the difference between ALL and ALLnoENSO.

in the SST anomalies in July 2017 (Fig. ES2e), which probably led to the intensification of PJ teleconnection and $Z'500_{diffP}$ and acted to increase the likelihood of occurrence of extreme event. It is expected that extremely prolonged cloudy and little sunshine days over northern Japan will happen more frequently due to the Okhotsk high intensified by human-induced warming in the future, although the results are based on a single model. Further investigation with other models is required.

CONCLUSIONS. The record prolonged low sunshine in northern Japan in early August of 2017 was mainly attributed to the persistent cold inflow along the anomalous cyclone over Japan, which is simultaneously induced by an extraordinary development of the Okhotsk high associated with blocking over eastern Siberia and the intraseasonal PJ teleconnection pat-

tern. Interestingly, it is found that this extreme event would hardly have occurred without anthropogenic warming, which is linked to increased probability of occurrence of extremely enhanced anticyclones in the Okhotsk Sea by 2.5–3.2 times due to human-induced warming. The 2017 decaying El Niño also increased the event occurrence through the amplification of tripolar pattern, although it was a smaller contribution than the human influence.

ACKNOWLEDGMENTS. This work was supported by the Program for Integrated Research Program for Advancing Climate Models (TOUGOU program) from the Ministry of Education, Culture, Sports, Science and Technology (MEXT), Japan. The MIROC5 simulations were performed using the Earth Simulator at JAMSTEC and the NEC SX at NIES.

REFERENCES

- Allen, M. R. 2003: Liability for climate change. *Nature*, **421**, 891–892, <https://doi.org/10.1038/421891a>.
- Arai, M., and M. Kimoto, 2008: Simulated interannual variation in summertime atmospheric circulation associated with the East Asian monsoon. *Climate Dyn.*, **31**, 435–447, <https://doi.org/10.1007/s00382-007-0317-y>.
- Christidis, N., and P. A. Stott, 2014: Change in the odds of warm years and seasons due to anthropogenic influence on the climate. *J. Climate*, **27**, 2607–2621, <https://doi.org/10.1175/JCLI-D-13-00563.1>.
- , M. McCarthy, A. Ciavarella, and P. A. Stott, 2016: Human contribution to the record sunshine of winter 2014/15 in the United Kingdom. *Bull. Amer. Meteor. Soc.*, **97**, S47–S50, <https://doi.org/10.1175/BAMS-D-16-0143.1>.
- Harada, Y., and Coauthors, 2016: The JRA-55 Reanalysis: Representation of atmospheric circulation and climate variability. *J. Meteor. Soc. Japan*, **94**, 269–302, <https://doi.org/10.2151/jmsj.2016-015>.
- Hirota, N., and M. Takahashi, 2012: A tripolar pattern as an internal mode of the East Asian summer monsoon. *Climate Dyn.*, **39**, 2219–2238, <https://doi.org/10.1007/s00382-012-1416-y>.
- Kamae, Y., M. Watanabe, M. Kimoto, and H. Shiogama, 2014: Summertime land–sea thermal contrast and atmospheric circulation over East Asia in a warming climate—Part I: Past changes and future projections. *Climate Dyn.*, **43**, 2553–2568, <https://doi.org/10.1007/s00382-014-2073-0>.
- Kimoto, M., 2005: Simulated change of the East Asian circulation under global warming scenario. *Geophys. Res. Lett.*, **32**, L16701, <https://doi.org/10.1029/2005GL023383>.
- Kobayashi, S., and Coauthors, 2015: The JRA-55 Reanalysis: General specifications and basic characteristics. *J. Meteor. Soc. Japan*, **93**, 5–48, <https://doi.org/10.2151/jmsj.2015-001>.
- Kodama, Y.-M., 1997: Airmass transformation of the Yamase air-flow in the summer of 1993. *J. Meteor. Soc. Japan*, **75**, 737–751, https://doi.org/10.2151/jmsj.1965.75.3_737.
- Kosaka, Y., and H. Nakamura, 2006: Structure and dynamics of the summertime Pacific–Japan teleconnection pattern. *Quart. J. Roy. Meteor. Soc.*, **132**, 2009–2030, <https://doi.org/10.1256/qj.05.204>.
- , and —, 2010: Mechanisms of meridional teleconnection observed between a summer monsoon system and a subtropical anticyclone. Part I: The Pacific–Japan pattern. *J. Climate*, **23**, 5085–5108, <https://doi.org/10.1175/2010JCLI3413.1>.
- Liebmann, B., and C. A. Smith, 1996: Description of a complete (interpolated) outgoing longwave radiation dataset. *Bull. Amer. Meteor. Soc.*, **77**, 1275–1277.
- Nakamura, H., and T. Fukamachi, 2004: Evolution and dynamics of summertime blocking over the Far East and the associated surface Okhotsk high. *Quart. J. Roy. Meteor. Soc.*, **130**, 1213–1233, <https://doi.org/10.1256/qj.03.101>.
- Nitta, T., 1987: Convective activities in the tropical western Pacific and their impact on the Northern Hemisphere summer circulation. *J. Meteor. Soc. Japan*, **65**, 373–390, https://doi.org/10.2151/jmsj.1965.65.3_373.
- Rayner, N. A., D. E. Parker, E. B. Horton, C. K. Folland, L. V. Alexander, D. P. Rowell, E. C. Kent, and A. Kaplan, 2003: Global analyses of sea surface temperature, sea ice, and night marine air temperature since the late nineteenth century. *J. Geophys. Res.*, **108**, 4407, <https://doi.org/10.1029/2002JD002670>.
- Sato, N., and M. Takahashi, 2007: Dynamical processes related to the appearance of the Okhotsk high during early midsummer. *J. Climate*, **20**, 4982–4994, <https://doi.org/10.1175/JCLI4285.1>.
- Shiogama, H., M. Watanabe, Y. Imada, M. Mori, M. Ishii, and M. Kimoto, 2013: An event attribution of the 2010 drought in the south Amazon region using the MIROC5 model. *Atmos. Sci. Lett.*, **14**, 170–175, <https://doi.org/10.1002/asl2.435>.
- , —, —, —, Y. Kamae, M. Ishii, and M. Kimoto, 2014: Attribution of the June–July 2013 heat wave in the southwestern United States. *SOLA*, **10**, 122–126, <https://doi.org/10.2151/sola.2014-025>.
- Takahashi, C., M. Watanabe, H. Shiogama, Y. Imada, and M. Mori, 2016: A persistent Japanese heat wave in early August 2015: Role of natural variability and human-induced warming [in “Explaining Extreme Events of 2015 from a Climate Perspective”]. *Bull. Amer. Meteor. Soc.*, **97**, S107–S112, <https://doi.org/10.1175/BAMS-D-16-0157.1>.
- Wakabayashi, S., and R. Kawamura, 2004: Extraction of major teleconnection patterns possibly associated with the anomalous summer climate in Japan. *J. Meteor. Soc. Japan*, **82**, 1577–1588, <https://doi.org/10.2151/jmsj.82.1577>.
- Watanabe, M., and Coauthors, 2010: Improved climate simulation by MIROC5: Mean states, variability, and climate sensitivity. *J. Climate*, **23**, 6312–6335, <https://doi.org/10.1175/2010JCLI3679.1>.

